

Article

Theoretical Investigation of the Adsorption of Cadmium Iodide from Water Using Polyaniline Polymer Filled with TiO₂ and ZnO Nanoparticles

Noureddine Mahdhi ^{1,*}, Norah Salem Alsaari ^{2,*}, Fatimah Mohammed Alzahrani ^{2,*},
Khadijah Mohammedsahle Katubi ^{2,*}, Abdelfattah Amari ^{3,4} and Saber Hammami ⁵

¹ Laboratory Materials Organizations and Properties, Tunis El Manar University, Tunis 2092, Tunisia

² Chemistry Department, College of Science, Princess Nourah Bint Abdulrahman University, Riyadh 11671, Saudi Arabia

³ Department of Chemical Engineering, College of Engineering, King Khalid University, Abha 61411, Saudi Arabia; Abdelfattah.amari@enig.rnu.tn

⁴ Research Laboratory of Energy and Environment, Department of Chemical Engineering, National School of Engineers, Gabes University, Gabes 6072, Tunisia

⁵ FEMTO-ST Institute, CNRS UMR-6174, Université de Bourgogne Franche-Comté, 25030 Besançon, France; saber.hammami@femto-st.fr

* Correspondence: noureddine.mahdhi@gmail.com (N.M.); nsalsaari@pnu.edu.sa (N.S.A.); fmalzahrani@pnu.edu.sa (F.M.A.); kmkatubi@pnu.edu.sa (K.M.K.)



Citation: Mahdhi, N.; Alsaari, N.S.; Alzahrani, F.M.; Katubi, K.M.; Amari, A.; Hammami, S. Theoretical Investigation of the Adsorption of Cadmium Iodide from Water Using Polyaniline Polymer Filled with TiO₂ and ZnO Nanoparticles. *Water* **2021**, *13*, 2591. <https://doi.org/10.3390/w13182591>

Academic Editor: Ivar Zekker

Received: 28 August 2021

Accepted: 16 September 2021

Published: 19 September 2021

Publisher's Note: MDPI stays neutral with regard to jurisdictional claims in published maps and institutional affiliations.



Copyright: © 2021 by the authors. Licensee MDPI, Basel, Switzerland. This article is an open access article distributed under the terms and conditions of the Creative Commons Attribution (CC BY) license (<https://creativecommons.org/licenses/by/4.0/>).

Abstract: The removal of heavy metals from drinking water has attracted great interest in water purification technology. In this study, a biocompatible Polyaniline (PANI) polymer filled with TiO₂ and ZnO nanoparticles (NPs) is considered as an adsorbent of cadmium iodide from water. Theoretical investigation of the van der Waals (vdW) interactions deduced from the Hamaker constant calculated on the basis of Lifshitz theory was presented. It was found that the surface energy as well as the work of adhesion between water and PANI/NPs across air increases with an increasing volume fraction of the TiO₂ and ZnO nanoparticles. Consequently, an increase in the Laplace pressure around the cavities/porosities was found, which leads to the enhancement of the specific contact surface between water and PANI/NPs. On the other hand, for the interactions between CdI₂ particles and PANI/NPs surface across water, we show that the interactions are governed principally by the attractive London dispersion forces. The vdW energy and force increase proportionally with the augmentation of the volume fraction of nanoparticles and of the radius of the CdI₂ particle. Particularly, the PANI/TiO₂ has been proved to be a better candidate for adsorption of cadmium iodide from water than PANI/ZnO.

Keywords: adsorption; polyaniline; cadmium iodide

1. Introduction

Cadmium metal has become a material that is inescapable for a wide variety of industrial applications such as batteries, alloys, coatings, solar cells, plastic stabilizers, and pigments [1–5]. These successful industrial features mask many environmental and health compatibility problems. Cadmium is non-biodegradable and hence, once released to the environment, it stays in circulation, especially in potable water and soil [6–8]. Cadmium iodide is one of the cadmium compound wastes. It can get into drinking water (groundwater or surface water) from the wastewater of electroplating industries and the manufacturing of phosphors [9–11]. In fact, such industries use an aqueous solution containing cadmium iodide Cd-I complexes such as CdI⁺, CdI₂, CdI₃[−], and CdI₄^{2−} as an electrolyte [12,13]. Humans get exposed to cadmium by ingestion (drinking or eating) or inhalation. Ailments such as bone disease, renal damage, and several forms of cancer are attributed to overexposure to cadmium [14]. For human health safety, the World Health Organization

(WHO) and other recent research bodies have provided the recommended permissible safe limit concentration of cadmium metal in drinking water and wastewater to be inferior to $0.003 \text{ mg}\cdot\text{L}^{-1}$ [15–17].

Recently, the removal of toxic heavy metals from water and soil has posed a great challenge for sustainable technologies. There are several types of physic-chemical treatments, such as adsorption, membrane filtration, electrodialysis, and photocatalysis [18]. Especially, the adsorption process has become one of the alternative techniques for wastewater purification due to its advantages regarding low cost, ease of operation, flexibility, and simplicity of design, and insensitivity to toxic pollutants [19]. Currently, many polymeric materials can be used as adsorbents because of their biocompatibility and wide range of porous structures that can be developed within the framework of a particular chemical system [19–21].

Polyaniline (PANI) is one of the most promising adsorbent polymers because of its low cost, ease of synthesis, good environmental stability, high electrical conductivity, ability to solubilize in various solvents, environmental steadiness, and exclusive redox properties [22–24]. Actually, many studies have been carried out to develop experimental procedures to synthesize a biocompatible PANI. Zhang [25] showed that preparing polyaniline with a higher molecular weight may be one of the methods to obtain polyaniline with good biocompatibility. Agilan [26] demonstrates that the incorporation of silver nanoparticles on PANI/TiO₂, fabricated by electropolymerization, enhances their biocompatibility.

However, for the adsorption application, many researchers have studied the effect of different types of dopants and/or composite of PANI polymer adsorption behavior [24,27]. It was demonstrated that the addition of zinc titanate (ZTO) nanoparticles to PANI by polymerization enhances the adsorption of congo red dye [22]. Zhu et al. [28] show that PANI/TiO₂ composite exhibits enhanced adsorption efficiency of formaldehyde and high stability compared to that of activated carbon. Khong [29] investigated the effect of incorporation of titanium dioxide (TiO₂) nanoparticles, single-walled carbon nanotube (SWNT), hexanoic acid (HA), and multi-walled carbon nanotube (MWNT) in polyaniline (PANI) nanocomposites for heavy metal removal application. They found that PANI/HA/TiO₂/MWNT showed the highest heavy metal removal efficiency.

Especially, the TiO₂ and ZnO fillers are the most used fillers for reinforcing many of the polymer matrices for many applications such as catalysis adsorption [30,31]. They exhibit many advantages such as an abundance in nature, biocompatibility, low-cost preparation with different sized and shaped particles (including nanowires, nanotubes, nanofibers, core-shell structures, and hollow nanostructures), photo-catalytic properties, antiseptic and antibacterial properties, and a higher surface energy which may result in a high degradation activity in adsorption [32,33].

On the other hand, the above-mentioned studies were studied adsorption without taking account of the effect of van der Waals (vdW) forces because of their weak nature, particularly in water, where the strength of the force is usually less than 1/100 of its strength in the air [34]. However, the vdW forces, which occur at long range (greater than 10 nm down to interatomic spacing about 0.2 nm), exhibit a very strong attraction between interacting particles. The main common example of this concept is the ability of geckos to maintain contact with the vertical wall surfaces. Theoretical estimation of the pertinent parameters of the adsorption such as vdW energy, and force, the work of adhesion is fundamental in the aim to predict a material adsorption behavior and to optimize the choice of the type and rate of dosing of each precursor of adsorbent.

Therefore, in this study, we reported a theoretical calculation of the van der Waals vdW interactions, using a Hamaker constant calculated on the basis of the Lifshitz macroscopic approach, with the aim to evaluate the pertinent parameter to the adsorption; the vdW energy, the vdW forces, the surface energy and the work of adhesion of interacting mediums. The second section describes the theoretical computational methods and materials data. The third deals with the determination of the dielectric permittivity as well as the refractive index of PANI/NPs as a function of volume fraction Φ of the nanoparticles and the study

of the effect of the volume fraction Φ and the type of nanoparticles filler on the vdW interactions between water and PANI/NPs in air. In the fourth section, we evaluate the vdW interactions between a spherical cadmium particle waste CdI_2 and the surface PANI/NPs in a water medium as an adsorption case study. The effect of the volume fraction, the type of nanoparticles filler, and the particle waste of CdI_2 on the vdW interactions is discussed. Section 4 presents the conclusions of this work.

2. Materials and Methods

2.1. Computational Methods

The computational method used in this study has been validated by many research works for evaluating the vdW interactions for adsorption studies for the diversity of materials liquids, solids, and gas. It has presented good accordance with experimental results [34–38].

2.1.1. VdW Interactions between Two Flat Surfaces across Air

VdW interactions are the principal driving interactions responsible for the adsorption phenomenon. They are responsible for the attractions between any two bodies because, while they are not as strong as Coulombic or H-bonding interactions, they are always present and can be important both at small and large separations [38] (pp. 107–130). Two flat surfaces interacting across the third medium, like the one that exists between the surface of PANI/NPs nanocomposites and water (Figure 1), involve vdW energy as given by the following equation [38] (p. 254):

$$U = \frac{-H}{12\pi x^2} \quad (1)$$

where x is the separating distance between two interacting mediums and H is the famous Hamaker constant.

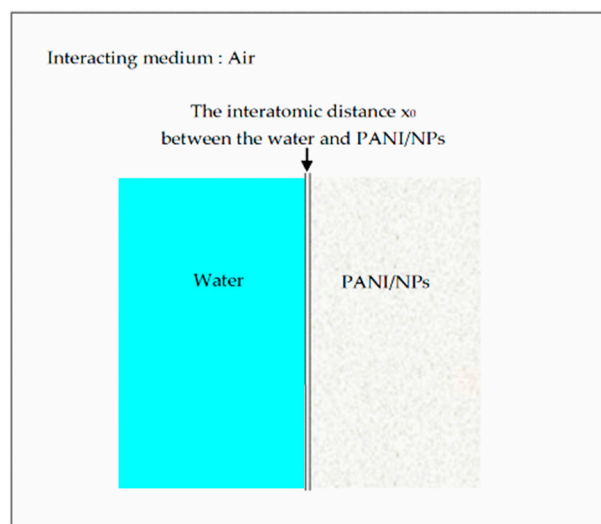


Figure 1. Water and PANI/NPs interacting in air at the separating cut off distance x_0 .

The surface energy γ of PANI/NPs can be evaluated from knowledge of the Hamaker constant H according to the relation [38] (p. 254):

$$\gamma = -\frac{H}{24 \cdot \pi \cdot x_0^2} \quad (2)$$

where x_0 is the cut-off which defines as the interatomic distance between the water and the PANI/NPs surface. It is typically equal to 0.165 nm. The distance x_0 yields values

for surface energy in such good agreement with those measured, even for very different liquids and solids [38] (p. 257).

2.1.2. Van der Waals Interactions between Spherical Particle and Flat Surface across Water

As a case study of the adsorption, we consider a spherical cadmium iodide CdI_2 particle of a radius R_c interacted with the flat surface of PANI/NPs over water medium at room temperature (298.15 K), as shown in Figure 2. The CdI_2 particle is subjected to the vdW interaction by the surface of PANI/NPs that can be attractive or repulsive. At a separating distance $x \ll R$ (in the range of 0.1–50 nm), the corresponding vdW energy is a function of the Hamaker constant H and the radius R_c of the particle of CdI_2 and the separating distance x as [38] (p. 254):

$$U = -\frac{H \cdot R_c}{6x} \quad (3)$$

The corresponding adhesion force F resulting from the vdW interaction is defined as the first derivative of the vdW energy as [38] (p. 254):

$$F(x) = -\frac{dU}{dx} = -\frac{H \cdot R_c}{6x^2} \quad (4)$$

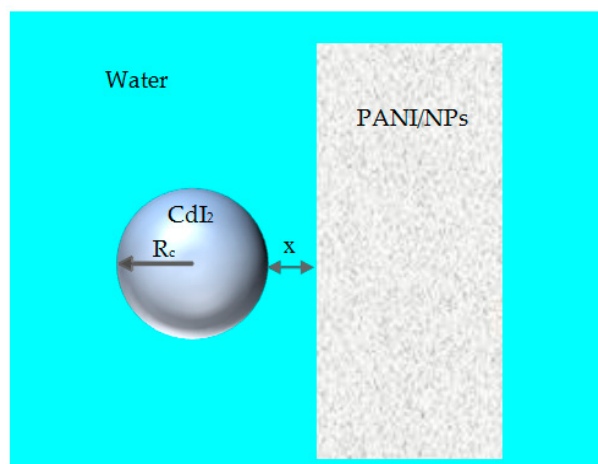


Figure 2. CdI_2 particle waste interacting with PANI/NPs across water under separating distance $x \ll R$.

In the aim to study the effect of particle size, we used two size particles of CdI_2 with radius $R_c = 136$ nm and $R_c = 348$ nm with known physical properties [11].

2.1.3. Method for Calculation of the Hamaker Constant

In the basis of the Lifshitz theory, the nonretarded Hamaker constant H between two mediums 1 and 2 interacting across medium 3 is expressed in terms of dielectric constant ϵ and the refractive index n [39]:

$$H = H^P + H^D \quad (5)$$

where the H^P is the polar component of the nonretarded Hamaker constant; it regroups the Keesom interaction that arises from permanent molecular dipoles and the Debye interaction that arises from permanent dipoles and induced dipoles [40–42]. It is expressed as function as dielectric permittivity by [38] (p. 260):

$$H^P = \frac{3}{4} K_B T \frac{\epsilon_1 - \epsilon_3}{\epsilon_1 + \epsilon_3} \cdot \frac{\epsilon_2 - \epsilon_3}{\epsilon_2 + \epsilon_3} \quad (6)$$

where k_B is the Boltzmann constant, T is the temperature, ϵ_1 , ϵ_2 , and ϵ_3 are the dielectric permittivity of the three interacting mediums.

The H^D regroups the London dispersion interactions between instantaneously induced dipoles. It is a function of the refractive index of the 3 interacting mediums and is given by [38] (p. 260):

$$H^D = \frac{3h\nu_e}{8\sqrt{2}} \frac{(n_1^2 - n_3^2)(n_2^2 - n_3^2)}{(n_1^2 + n_3^2)^{0.5}(n_2^2 + n_3^2)^{0.5} \left[(n_1^2 + n_3^2)^{0.5} + (n_2^2 + n_3^2)^{0.5} \right]} \quad (7)$$

ν_e is the main electronic absorption frequency in the UV, typically around $3 \times 10^{15} \text{ s}^{-1}$ [38] (p. 260), h is the Planck constant, and (n_1, n_2, n_3) are respectively the refractive indexes which are visible (water, sample, air).

For metals, the dielectric constant is very high as infinite, and then we may neglect the contribution of the term $(\epsilon_1 - \epsilon_2)/(\epsilon_1 + \epsilon_2)$ in Equation (3). Therefore, the polar component of the nonretarded Hamaker constant H^P is function only of the dielectric constants and temperature, and is simplified as follows [43]:

$$H^P = \frac{3}{4} K_B T \left(\frac{\epsilon_2 - \epsilon_3}{\epsilon_2 + \epsilon_3} \right) \quad (8)$$

2.1.4. Model for Calculation the Dielectric Constant of Nanocomposites

In this study, the pure PANI polymer and the PANI filled by the nanoparticles of TiO_2 and ZnO with volume fraction $\Phi = (20\%, 40\%, 60\%, 80\%)$ are used.

To calculate the dielectric constant of the nanocomposites, the power-law model was used, considering that the spherical particle filler is uniformly dispersed in a continuous PANI matrix [44].

$$\epsilon_c^{1/3} = \Phi \epsilon_m^{1/3} + (1 - \Phi) \epsilon_f^{1/3} \quad (9)$$

where Φ is the filler volume fraction (%), ϵ_c , ϵ_m , and ϵ_f are de dielectric constant respectively of the nanocomposite (PANI/NPs), the polymer matrix (PANI), and the nanoparticles filler (NPs of TiO_2 and ZnO).

2.1.5. Models for Calculation of the Refractive Index

The calculation of the refractive index for PANI/NPs was done referring to the pioneering work the most popular mixing theory of Maxwell garnet [45]:

$$n_c^2 = n_m^2 \frac{(n_f^2 + 2n_m^2) + 2\Phi(n_f^2 - n_m^2)}{(n_f^2 + 2n_m^2) - \Phi(n_f^2 - n_m^2)} \quad (10)$$

where Φ is the filler volume fraction (%), n_c , n_m and n_f are the refractive indexes respectively of nanocomposites (PANI/NPs), matrix (PANI), and NPs filler (TiO_2 and ZnO).

2.2. Materials

The theoretical calculations of the nonretarded Hamaker constant on the basis of the Lifshitz theory provide a known dielectric constant and the refractive index of the three interacting materials. Table 1 summarizes the dielectric constants and the refractive indexes of the PANI, the NPs of TiO_2 and ZnO , water, and CdI_2 particle considered in this study. The values of the dielectric constants were taken at 1 MHz. Where, the refractive indexes were taken at visible wavelength 600 nm.

Table 1. Dielectric constants and refractive indexes of the mediums at room temperature (298.15 K) considered in this study.

Material	Dielectric Constant at 1 MHz	Refractive Index at 600 nm
PANI	68 [46]	1.51 [47]
TiO ₂ (anatase) [48]	86	2.6
ZnO [48]	8.5	2
Water [49]	78.4	1.33
CdI ₂ (R = 348 nm) [11]	-	2.145
CdI ₂ (R = 136 nm) [11]	-	2.1

3. Results and Discussion

All calculations and discussions of the results using computational method are carried out at room temperature (298.15 K).

3.1. Dielectric Permittivity and Refractive Index of PANI/NPs: Effect of NPs Type and Rate

Table 2 reports the value of the dielectric constant ϵ and the refractive index n of nanocomposites PANI/NPs with the correspondent volume fraction Φ of TiO₂ and ZnO nanoparticles using Equations (9) and (10). The ϵ of PANI/TiO₂ increases with the volume fraction Φ of TiO₂ NPs. However, the ϵ for PANI/ZnO decreases with the volume fraction Φ of ZnO NPs. This result is attributed to the high dielectric constant of TiO₂ NPs rather than the pure PANI and the less dielectric constant of the ZnO NPs. However, due to the higher refractive index of NPs compared with the pure PANI, we find that the refractive indexes n of PANI/TiO₂ and PANI/ZnO increases with the increasing the volume fraction Φ of NPs. The comparison of n values visualized in the table affirms that the PANI/TiO₂ exhibits a higher refractive index than those for PANI/ZnO.

Table 2. The dielectric constant and the refractive index of PANI/NPs as a function of volume fraction Φ of NPs at room temperature (298.15 K).

Φ	PANI/TiO ₂		PANI/ZnO	
	ϵ	n	ϵ	n
0	68	1.51	68	1.51
0.2	71.3765	1.69352	49.5720	1.60203
0.4	74.8631	1.88852	34.8160	1.69644
0.6	78.4613	2.10002	23.3240	1.79379
0.8	82.1730	2.33429	14.6880	1.89476

3.2. VdW Interaction between PANI/NPs and Water across Air

This part of the study reports a prediction and evaluation of the type of the vdW interactions (attractive or repulsive) between water and PANI/NPs across air using the computational methods as described in Section 2.1.1. Figure 3 reports the values of the nonretarded Hamaker constants H , H^P , and H^D between PANI/NPs and water across air as function as the volume fraction Φ of the NPs calculated using Equations (5)–(7). It is remarked that all values of nonretarded Hamaker constants are positives, suggesting that the interactions of PANI/NPs and water across air are always attractive for the two types of NPs—TiO₂ and ZnO—and at all volume fraction Φ of NPs. However, for the same Φ , a higher dominance (>94%) of the dispersive nonretarded Hamaker constant H^D in the total value of Hamaker constant H is observed. This result was particularly relevant because it affirms the dominance of vdW dispersive attractions between water and PANI/NPs across the air.

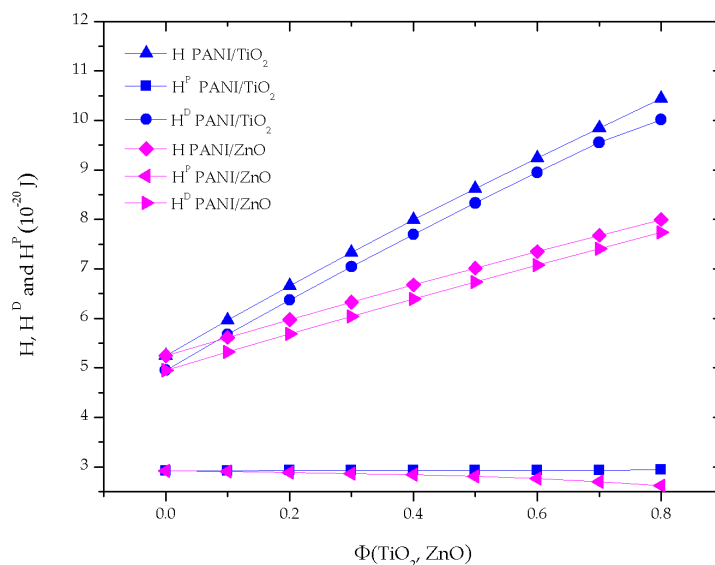


Figure 3. The nonretarded Hamaker constants as a function of the volume fraction Φ of NPs for PANI/NPs-Water across air.

Figure 4 illustrates the vdW energy for PANI/TiO₂ and PANI/ZnO at the interatomic distance $x_0 = 0.165$ nm. We find that the vdW energy is much higher, with an increasing volume fraction Φ of NPs, and this fact is remarkable for PANI/TiO₂. This result reflects that the TiO₂ NPs is better than ZnO NPs for enhancing the vdW attractive energy between water and PANI/NPs.

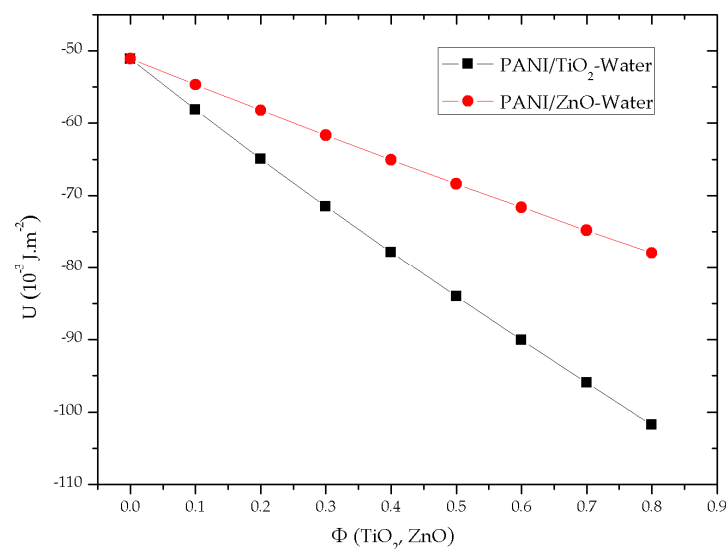


Figure 4. VdW energy U between PANI/NPs-Water across air as a function of the volume fraction Φ of TiO₂ and ZnO NPs.

Figure 5 depicts the evolution of the surface energy of two composite PANI/NPs for various Φ calculated using Equation (2). The surface energy range values $(25\text{--}60) \times 10^{-3} \text{ J.m}^{-1}$ are in good agreement with those reported by many studies [50,51], which shows the accuracy of the calculation method. As already expected from the Hamaker constant evolution, the surface energy was increasing with the volume fraction Φ for two PANI/NPs except the polar part γ^P for PANI/ZnO because of the decrease in their dielectric constant with the volume fraction Φ (Table 1).

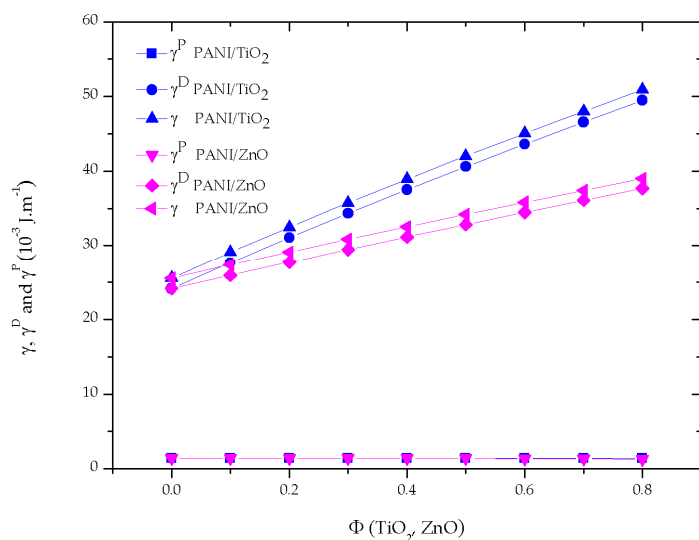


Figure 5. Surface energy of PANI/TiO₂ and PANI/ZnO as a function of Φ of NPs.

As expected from the Hamaker constant behavior, the PANI/TiO₂ composites exhibit higher surface energy values for all volume fractions Φ of NPs. This is attributed to the higher dielectric constant and the refractive index of the PANI/TiO₂.

It is noticeable that for the two PANI/TiO₂ and PANI/ZnO, the surface energy is dominated principally by their dispersive γ^D part, which represents >94% in the total surface energy γ . For such cases, the work of adhesion W_A between PANI/NPs and water is approximated as [52]:

$$W_A = 2 \left(\sqrt{\gamma_1^D \gamma_2^D} + \sqrt{\gamma_1^P \gamma_2^P} \right) \tag{11}$$

where γ_1^D and γ_2^D represent respectively the polar part of the surface energy of PANI/NPs and water. is typically equal to $19.9 \times 10^{-3} \text{ N.m}$ [52].

As already expected from Figure 6, the work of adhesion W_A between PANI/NPs-Water across air increases with the volume fraction Φ of NPs and the highest adhesion occurs between PANI/TiO₂-Water. Therefore, it is well known that the nanoparticles filler enhances the adhesion between PANI/NPs and water, and the adhesion is involved principally in the London dispersion forces.

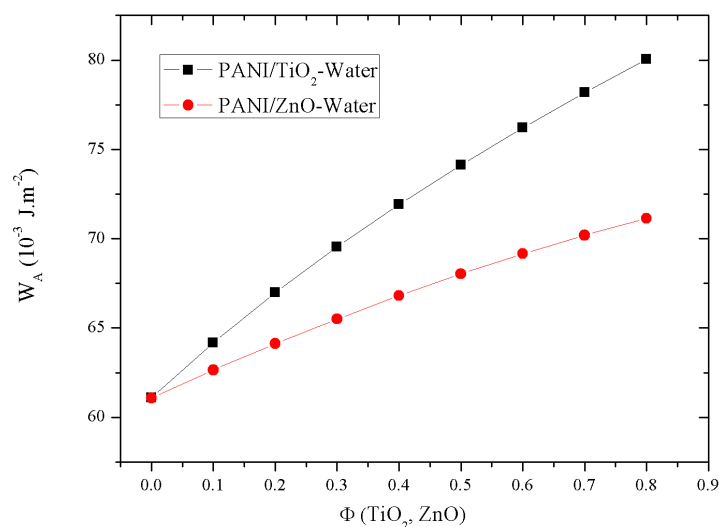


Figure 6. Work of adhesion of PANI/TiO₂ and PANI/ZnO as a function of the volume fraction Φ of NPs.

As mentioned previously in this section, we have shown that the PANI/NPs-water interactions at the interatomic distance x_0 was enhanced with the increase in the rate of volume fraction Φ of NPs.

Generally, the common adsorbent materials present much nano and micro porosity architecture; this porosity gives rise to a significant Laplace pressure that drives the interface in the concave direction, and then it is responsible for the driving water in the cavities as mentioned in Figure 7. This fact leads to an increase in the specific contact surface, and then the adsorption of waste from water in the cavities can be enhanced.

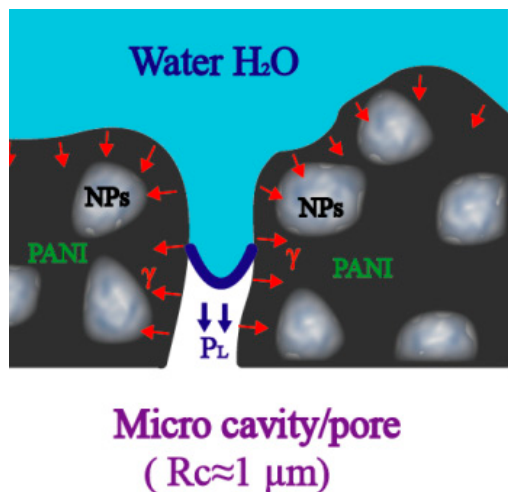


Figure 7. Schematic illustration of the penetration of water on the cavity/pore of PANI/NPs described by the Laplace pressure.

The Laplace pressure is expressed as a function of surface energy γ and the cavity radius R_c as:

$$P_L = \frac{\gamma}{R_c} \tag{12}$$

Figure 8 reports the evolution of the Laplace pressure for typical size cavity radius $R_c = 100 \mu\text{m}$.

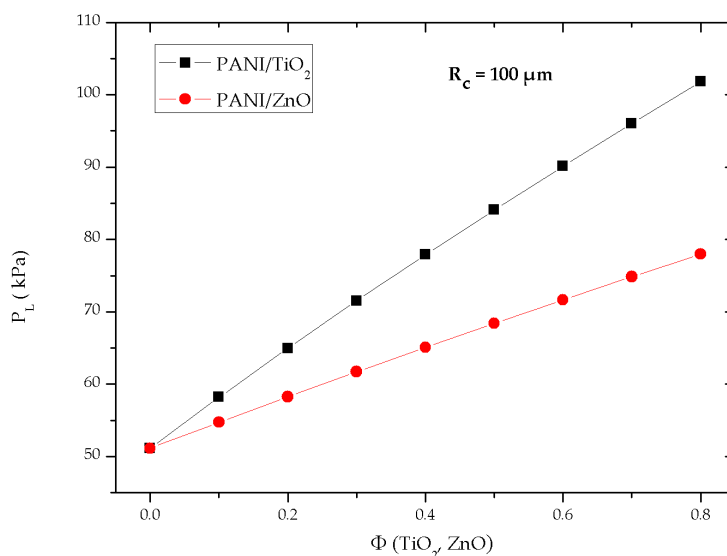


Figure 8. Laplace pressure on PANI/TiO₂ and PANI/ZnO cavity, with $R_c = 1 \mu\text{m}$, as function of the volume fraction Φ of NPs.

The attraction around the cavities/porosities caused by Laplace pressure is enhanced by incorporation of NPs. We compute that this finding enhances the specific contact surface and then the adsorption of particle waste from water in the contact by considering the contribution of the Laplace pressure.

3.3. Interaction between Spherical CdI₂ Particle Waste and Surface of PANI/NPs across Water

3.3.1. The Nonretarded Hamaker Constants Behavior

We illustrate the interaction between cadmium iodide CdI₂ (medium 1) and PANI/NPs (medium 2) across water (medium 3), as shown in Figure 2 at room temperature (298.15 K).

Tables 3 and 4 summarize the nonretarded Hamaker constants H , H^P , and H^D , for the interactions between the spherical particle of CdI₂ and the flat surface of PANI/NPs nanocomposites across water. The calculation was done using Equations (5)–(8) for the two CdI₂ radius particle $R_c = 136$ nm and $R_c = 348$ nm and for various volume fractions (0, 20%, 40%, 60%, and 80%) of NPs of TiO₂ and ZnO.

Table 3. The nonretarded Hamaker constants as a function of the volume fraction Φ of NPs for PANI/TiO₂- CdI₂ across water: (a) $R_c = 136$ nm, (b) $R_c = 348$ nm.

Φ (TiO ₂)	$R_c = 348$ nm			$R_c = 136$ nm		
	H^P (10 ⁻²⁰ J)	H^D (10 ⁻²⁰ J)	H (10 ⁻²⁰ J)	H^P (10 ⁻²⁰ J)	H^D (10 ⁻²⁰ J)	H (10 ⁻²⁰ J)
0	-0.02193	3.3126	3.14127	-0.02193	3.1632	3.14127
0.2	-0.01477	6.4547	4.62695	-0.01477	6.1619	6.14713
0.4	-0.00712	9.5229	6.08885	-0.00712	9.0885	9.08138
0.6	0.00024	12.545	7.53285	0.00024	11.969	11.96924
0.8	0.00725	15.549	8.9665	0.00725	14.83	14.83725

Table 4. The nonretarded Hamaker constants as a function of the volume fraction Φ of NPs for PANI/ZnO- CdI₂ across water for (a) $R_c = 136$ nm, (b) $R_c = 348$ nm.

Φ (ZnO)	R (CdI ₂) = 348 nm			R (CdI ₂) = 136 nm		
	H^P (10 ⁻²⁰ J)	H^D (10 ⁻²⁰ J)	H (10 ⁻²⁰ J)	H^P (10 ⁻²⁰ J)	H^D (10 ⁻²⁰ J)	H (10 ⁻²⁰ J)
0	-0.02193	3.3126	3.29067	-0.02193	3.1632	3.14127
0.2	-0.069547	4.9191	4.84955	-0.06954	4.6965	4.62695
0.4	-0.11885	6.5027	6.38385	-0.11885	6.2077	6.08885
0.6	-0.16715	8.0670	7.89985	-0.16715	7.7000	7.53285
0.8	-0.21130	9.6165	9.4052	-0.21130	9.1778	8.9665

The values of the nonretarded Hamaker constants are located in the range of most condensed phases (0.4–410⁻²⁰ J), which shows the accuracy of our calculation [38] (p. 255). The dispersive nonretarded Hamaker constant H^D is positive and represents 99% of the total nonretarded Hamaker constant H . Therefore, we have led to the important ascertainment that the interaction between CdI₂ particle and PANI/NPs across water is always attractive ($H > 0$) and is governed essentially by the London disperse vdW forces. Whereas, the H^P is negative and contributes about 1% in the total H value and then their repulsive effect on the vdW interactions can be neglected. Considering Equation (8), the negative value of H^P is attributed to the lower dielectric constant of PANI/NPs to the dielectric constant of water ($\epsilon = 78.1$), except for ($\epsilon(\text{PANI/TiO}_2)$) at ($\Phi = 0.6$ –0.8).

Consequently, these findings imply that the interactions between the spherical particle of CdI₂ and the flat surface of PANI/NPs nanocomposites across water are attractive. Note that the dispersive interactions depend only on the orbiting electron frequency, ν , and the refractive index, n (of the three interacting mediums), which are independent

of temperature; we reveal that the attraction between CdI₂ and PANI/NPs is always admissible for the functional temperature around the ambient temperature.

Note that the dispersive nonretarded Hamaker constant H^D is proportional to the refractive index of the mediums (Equation (7)), we found an increase of the nonretarded Hamaker constant H with increasing the volume filler fraction Φ and the refractive index of the CdI₂ particle. Interestingly, the increase in the vdW attraction was greater for TiO₂ NPs compared to that for ZnO.

3.3.2. VdW Energy

To evaluate the energy of the adsorption of the CdI₂ particle on the PANI/NPs surface from the water medium, we have computed the vdW energy given by relation (3) for the various volume fraction Φ of NPs and CdI₂ particle radius R_c . We have scaled the vdW energy to the $k_B T_{\text{room}}$ ($T_{\text{room}} = 298.15$ K) to quantify the strength of the vdW energy along the separating distance x . As illustrated in Figure 9, the behavior of the vdW energy versus the separating distance x is typically for attractive energy curves. At the nonretarded regime ($x < 20$ nm), the vdW energy curve undergoes asymptotic growth at around $U = -800 k_B T_{\text{room}}$ (for $x = 1.4$ nm), this behavior was found independently of the volume fraction Φ of NPs and of the radius R_c of the CdI₂ particle. This finding supports that the vdW energy is sufficiently strong at a small distance from PANI/NPs.

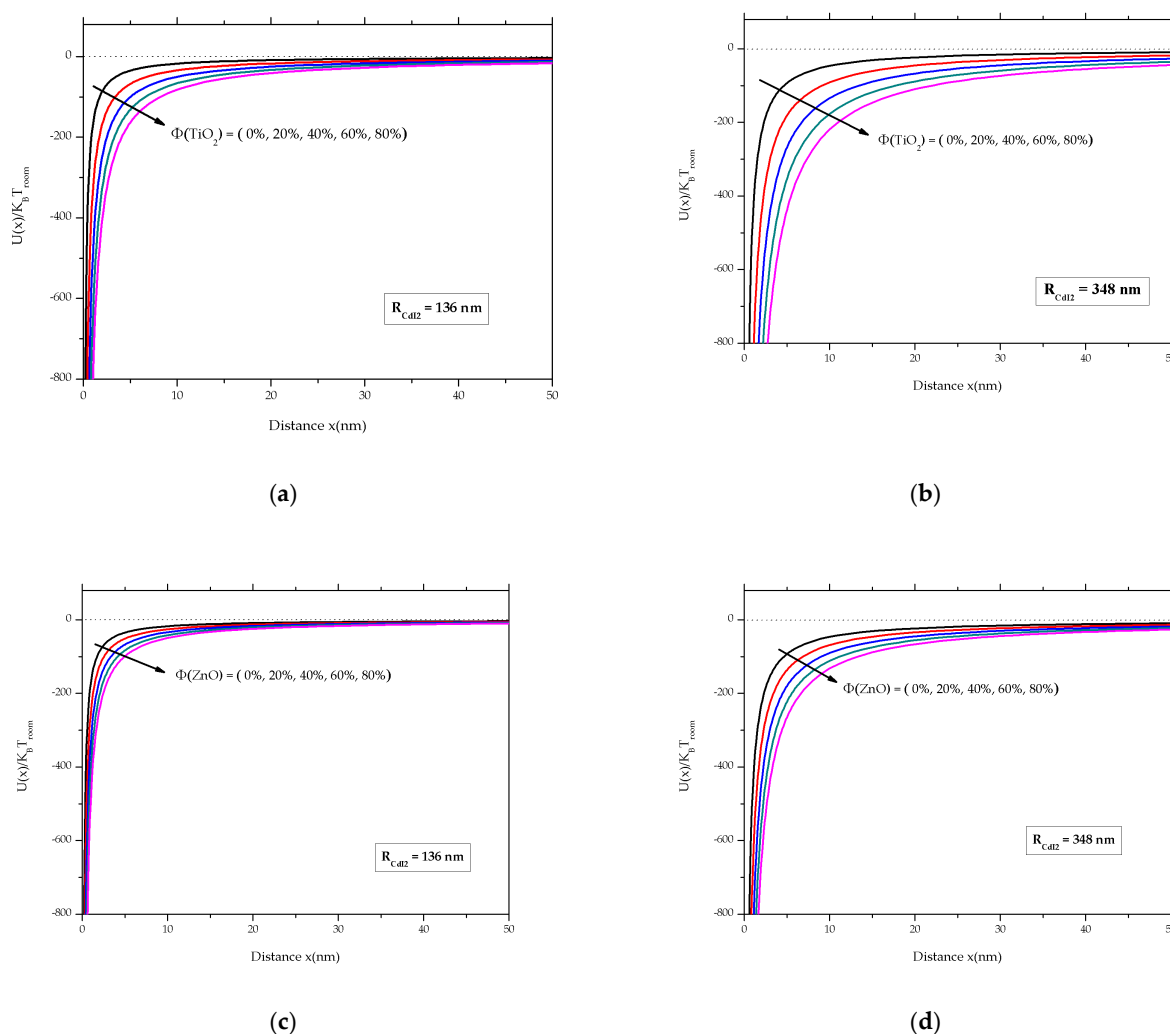


Figure 9. VdW energy U of CdI₂-PANI/NPs across water medium as function of separating distance x and for the various volume fraction Φ of NPs: (a) PANI/TiO₂ with $R_c = 136$ nm, (b) PANI/TiO₂ with $R_c = 348$ nm, (c) PANI/ZnO with $R_c = 136$ nm and (d) PANI/ZnO with $R_c = 348$ nm.

Compared to PANI/ZnO-CdI₂ (Figure 9c,d), the PANI/TiO₂-CdI₂ (Figure 9a,b) exhibits a higher vdW energy throughout the separating distance x (0–50 nm), which is caused by the higher refractive index of TiO₂ to that for ZnO NPs. Hence, the incorporation of the TiO₂ NPs leads to an increasing attraction, and then we show that TiO₂ NPs are better than ZnO NPs for enhancing the London attraction energy between CdI₂ particles and PANI/NPs nanocomposites across water medium.

Furthermore, as can be predicted from Equation (3), the vdW energy for the same type of NPs (Figure 9a–d) increased by increasing the radius R_c of the CdI₂ particles.

3.3.3. VdW Force–Distance Curves

The vdW forces F between CdI₂-PANI/NPs across water was calculated along the separating distance x (0.1–50 nm) using Equation (4). As illustrated in Figure 10, the vdW force–distance curves show a typically attractive behavior. For the nonretarded regime (approximately for $x < 20$ nm), we observe a dispersion in the force–distance curve (noted in Figure 10a increase of the vdW forces). The shape of this dispersion increases with the volume fraction Φ of the NPs and the particle radius R_c of the CdI₂.

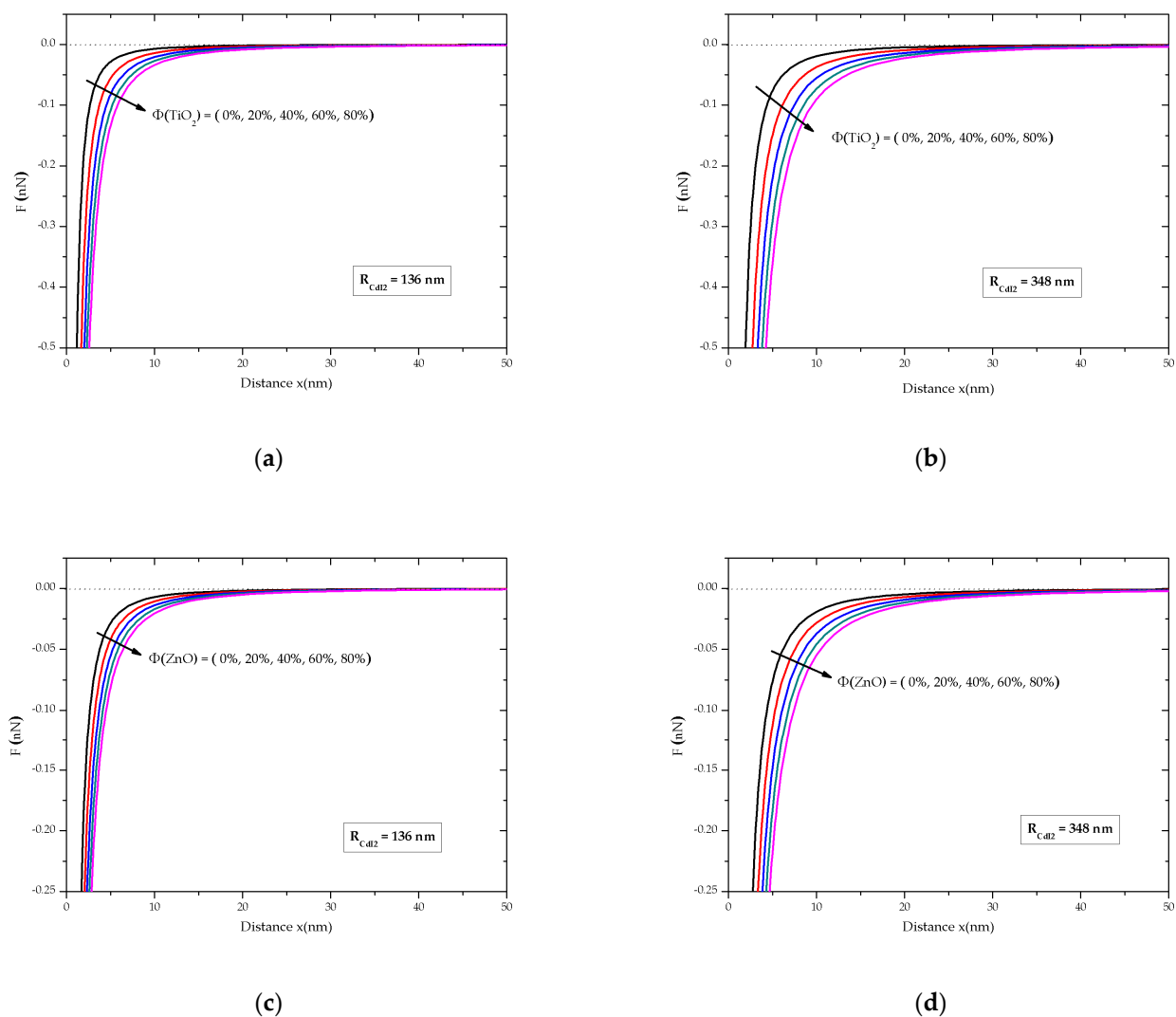


Figure 10. VdW forces F between CdI₂ and PANI/NPs across water medium as a function of the separating distance x and for Table 2. (a) PANI/TiO₂ with $R_c = 136$ nm, (b) PANI/TiO₂ with $R_c = 348$ nm, (c) PANI/ZnO with $R_c = 136$ nm and (d) PANI/ZnO with $R_c = 348$ nm.

Furthermore, the vdW force curves become stronger with the decreasing x , and this finding additionally supports that vdW attractions are the foremost driving force for particle adsorption at a long-range distance ($x < 10$ nm).

Thereby, taking account these above-mentioned findings, the vdW force and energy between CdI₂ particle and PANI/NPs surfaces across water are enhanced by increasing the volume fraction Φ of NPs and the radius R_c of the CdI₂ particle. Moreover, we can emphasize the advantageous effect of metal oxide nanoparticle filler (TiO₂ and ZnO) for improving the adsorption efficiency of the PANI matrix (unfilled).

3.3.4. Effect of the Nanoparticle Type

In the aim of evaluating the pertinent nanoparticles that mostly enhance the attractive vdW forces and energy, we have scaled the vdW force and energy of the PANI/NPs to those for pure PANI for the two-particle radius $R_c = 1.36$ nm and $R_c = 348$ nm. From relations (3) and (4), the scaled vdW force and energy depend only on the values of the Hamaker constant of pure and filled PANI as:

$$\frac{F_{\text{PANI/NPs}}}{F_{\text{PANI}}} = \frac{U_{\text{PANI/NPs}}}{U_{\text{PANI}}} = \frac{H_{\text{PANI/NPs}}}{H_{\text{PANI}}} \quad (13)$$

We have drawn the evolution of the scaled vdW and energy as a function of volume fraction Φ of NPs. As illustrated in Figure 11, the curves undergo a linear law of the form:

$$\frac{F_{\text{PANI/NPs}}}{F_{\text{PANI}}} = \frac{U_{\text{PANI/NPs}}}{U_{\text{PANI}}} = a + b \cdot \Phi \quad (14)$$

where a and b present the intercept and slope of the curves that describe the magnitude of the regression of the scaled vdW energy and force.

As clearly illustrated in Table 5, the slope for the PANI/TiO₂ is about two times higher than for PANI/ZnO. Thus, through this approach, we can demonstrate that the TiO₂ NP is the performer filler for enhancing the vdW energy and force that governed the adsorption of CdI₂ particle on PANI/TiO₂ surface from water.

Table 5. Fitting results of curves in Figure 11 using Equation (14).

Material	Intercept a	Standard Error	Slope b	Standard Error
PANI/TiO ₂	1.040	0.00928	4.609	0.01694
PANI/ZnO	1.014	0.00392	2.302	0.00716

Regarding the nonretarded Hamaker constant for the interaction between CdI₂ particles and PANI/NPs across water is mostly a function of the refractive index of the mediums, and therefore the enhancement on the magnitude of the nonretarded Hamaker constant is relative to the refractive index of the NP filler. Furthermore, the refractive index of NPs are higher and the magnitude of the attractive vdW interactions increase. Therefore, based on the theoretical analysis mentioned above, we can deduce that the adsorption of heavy metals on polymer composite from water can be improved by choosing the NP filler that exhibits the higher refractive index.

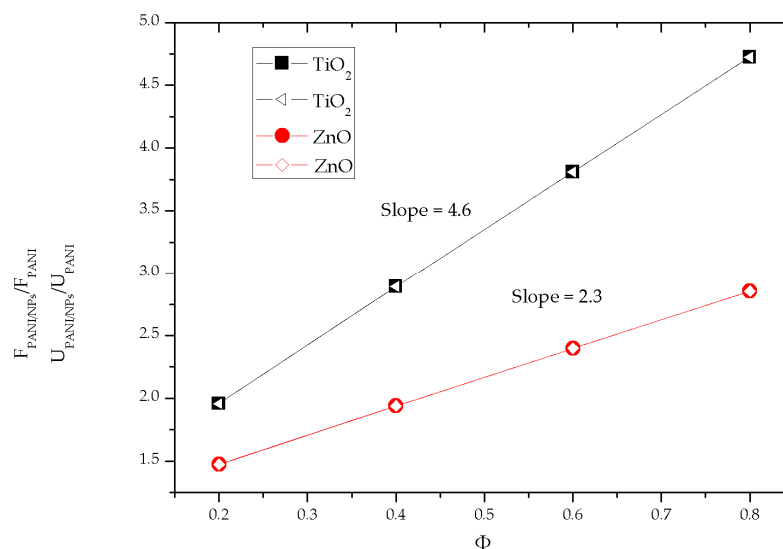


Figure 11. The scaled vdW energy and force of PANI/NPs to those of pure PANI.

In future research, we envisage the study of the effect of the temperature on the vdW interactions using the subjected model. Furthermore, these theoretical recommendations can be exploited experimentally on the study of the removal of the heavy metals from water on the PANI/NPs adsorbent.

4. Conclusions

The vdW interaction that governed adsorption was investigated from the theoretical calculation of the nonretarded Hamaker constant on the basis of the Lifshitz macroscopic approach. For the interaction between water and PANI filled with TiO₂ and ZnO NPs across air, we demonstrate that the surface energy of PANI/NPs, as well as the work of adhesion between water and PANI/NPs across water, increase with the increasing volume fraction Φ of TiO₂ and ZnO NPs. Consequently, an increase in the Laplace pressure around the cavities/porosities is found. We suggest that this finding is responsible for an increase in the specific contact surface between water and PANI/NPs and then enhance the adsorption capacity of the PANI/NPs.

However, the adsorption behavior of CdI₂ particles on the PANI/NP surface across water was explained in terms of the vdW energy and force. The results demonstrate that the vdW interactions are mostly governed by the London dispersion forces. At the nonretarded regime, the vdW energy and force increase strongly, indicating that vdW attraction is the most driving force for particle adsorption. We have demonstrated that an increase in the volume fraction Φ of TiO₂ and ZnO NPs and the radius of CdI₂ particles leads to an enhancement of the attractive vdW energy and forces between CdI₂ particles and PANI filled with TiO₂ and ZnO NPs across water. From scaling results, the TiO₂ NPs are better than ZnO NPs for enhancing the attractive vdW energy and force that governed adsorption of the CdI₂ particle on the PANI surface from the water. This fact is explained by the higher refractive index of the TiO₂ NPs that is relative to their London dispersion forces.

Collectively, considering that the vdW interaction is mostly governed by the dispersion London forces, the enhancement of the adsorption of nanocomposites can be done by choosing the NP filler with a higher refractive index rather than of the polymer matrix.

These results can be generalized for all other heavy metals that exhibit a refractive index in the vicinity of that for cadmium iodide.

Author Contributions: Conceptualization, methodology, investigation, writing—original draft, and review of the final manuscript: N.M., N.S.A., F.M.A., K.M.K.; formal analysis: resources, supervision, review and visualization: A.A., S.H.; review and editing: N.M., N.S.A., F.M.A., K.M.K.; resources and review, A.A., S.H. All authors have read and agreed to the published version of the manuscript.

Funding: This research was funded by the Deanship of Scientific Research at King Khalid University. Also, this research was funded by the Deanship of Scientific Research at Princess Nourah bint Abdulrahman University through the Fast-track Research Funding Program.

Institutional Review Board Statement: Not applicable.

Informed Consent Statement: Not applicable.

Data Availability Statement: Not applicable.

Acknowledgments: The authors extend their appreciation to the Deanship of Scientific Research at King Khalid University for funding this work through the research groups program under grant number RGP.1/111/42. Additionally, this research was funded by the Deanship of Scientific Research at Princess Nourah bint Abdulrahman University through the Fast-track Research Funding Program.

Conflicts of Interest: The authors declare no conflict of interest.

References

- Galushkin, N.E.; Yazvinskaya, N.N.; Galushkin, D.N. Nickel-cadmium batteries with pocket electrodes as hydrogen energy storage units of high-capacity. *J. Energy Storage* **2021**, *39*, 102597. [[CrossRef](#)]
- Badawi, A.; Al-Gurashi, W.; Al-Baradi, A.M.; Al-Hosiny, N. Alloying cadmium cobalt sulfide quantum dots for solar cells applications. *Mater. Sci. Semicond. Process.* **2019**, *95*, 1–6. [[CrossRef](#)]
- Lohitha, B.; Thanikaikarasan, S.; Marjorie, S.R. Structural and optical properties of electroplated Cadmium Sulphide thin films. *Mater. Today Proc.* **2020**, *33 Pt 7*, 3405–3408. [[CrossRef](#)]
- Shah, D.K.; Devendra, C.K.; Muddassir, M.; Akhtar, M.S.; Kim, C.Y.; Yang, O.B. A simulation approach for investigating the performances of cadmium telluride solar cells using doping concentrations, carrier lifetimes, thickness of layers, and band gaps. *Sol. Energy* **2021**, *216*, 259–265. [[CrossRef](#)]
- Liu, H.; Liu, K.; Fu, H.; Ji, R.; Qu, X. Sunlight mediated cadmium release from colored microplastics containing cadmium pigment in aqueous phase. *Environ. Pollut.* **2020**, *263 Pt A*, 114484. [[CrossRef](#)]
- Gupta, T.; Agarwal, A.K.; Agarwal, R.A.; Labhsetwar, N.K. *Environmental Contaminants: Measurement, Modelling and Control*; Energy, Environment, and Sustainability Series; Springer: Singapore, 2018; 322p, ISBN 13: 9789811073328.
- Han, Y. *Advances in Energy and Environmental Materials*; Springer Proceedings in Energy Series; Springer: Singapore, 2018; p. 760. [[CrossRef](#)]
- Asrari, E. *Heavy Metal Contamination of Water and Soil: Analysis, Assessment, and Remediation Strategies*, 1st ed.; Apple Academic Press: New York, NY, USA, 2014; pp. 1–129. [[CrossRef](#)]
- Ojo, A.A.; Dharmadasa, I.M. Electroplating of Semiconductor Materials for Applications in Large Area Electronics: A Review. *Coatings* **2018**, *8*, 262. [[CrossRef](#)]
- Chauré, N.; Samantilleke, A.P.; Dharmadasa, I. The effects of inclusion of iodine in CdTe thin films on material properties and solar cell performance. *Sol. Energy Mater. Sol. Cells* **2003**, *77*, 303–317. [[CrossRef](#)]
- Yahia, I.; Shapaan, M.; Ismail, Y.A.; Aboraia, A.; Shaaban, E. Thickness dependence of structural and optical properties of cadmium iodide thin films. *J. Alloys Compd.* **2015**, *636*, 317–322. [[CrossRef](#)]
- Paterson, R.; Anderson, J.; Anderson, S.S.; Lutfullah. Transport in aqueous solutions of group IIB metal salts (298.15 K). Part 3.—Isotopic diffusion coefficients for cadmium-115 ions in aqueous cadmium iodide. *J. Chem. Soc. Faraday Trans. 1 Phys. Chem. Condens. Phases* **1978**, *74*, 93–102. [[CrossRef](#)]
- Paterson, R.; Devine, C. Transport in aqueous solutions of group IIB metal salts. Part 7—Measurement and prediction of isotopic diffusion coefficients for iodide in solutions of cadmium iodide. *J. Chem. Soc. Faraday Trans. 1 Phys. Chem. Condens. Phases* **1980**, *76*, 1052–1061. [[CrossRef](#)]
- Saini, S.; Dhania, G. Cadmium as an Environmental Pollutant: Ecotoxicological Effects, Health Hazards, and Bioremediation Approaches for Its Detoxification from Contaminated Sites. In *Bioremediation of Industrial Waste for Environmental Safety*; Bharagava, R., Saxena, G., Eds.; Springer: Singapore, 2020. [[CrossRef](#)]
- WHO. *Guidelines for Drinking-Water Quality*, 4th ed.; Library Cataloguing-in-Publication Data; World Health Organization (WHO): Geneva, Switzerland, 2011; 180p, ISBN 978 92 4 154815 1.
- Shrestha, R.; Ban, S.; Devkota, S.; Sharma, S.; Joshi, R.; Tiwari, A.P.; Joshi, M.K. Technological trends in heavy metals removal from industrial wastewater: A review. *J. Environ. Chem. Eng.* **2021**, *9*, 105688. [[CrossRef](#)]
- O’Melia, C.R. Interface Science in Drinking Water Treatment Theory and Application: Chapter 18—Fundamentals of particle Stability. In *Interface Science and Technology*; Newcombe, G., Dixon, D., Eds.; Elsevier: Amsterdam, The Netherlands, 2006; Volume 10, pp. 317–362. [[CrossRef](#)]
- Barakat, M.A. New trends in removing heavy metals from industrial wastewater. *Arab. J. Chem.* **2011**, *4*, 361–377. [[CrossRef](#)]
- Nasar, A.; Mashkoo, F. Application of polyaniline-based adsorbents for dye removal from water and wastewater—A review. *Environ. Sci. Pollut. Res.* **2019**, *26*, 5333–5356. [[CrossRef](#)]

20. Prabhakar, P.K.; Raj, S.; Anuradha, P.; Sawant, S.N.; Doble, M. Biocompatibility studies on polyaniline and polyaniline–silver nanoparticle coated polyurethane composite. *Colloids Surfaces B Biointerfaces* **2011**, *86*, 146–153. [CrossRef] [PubMed]
21. Prabhu, R.; Jeevananda, T.; Reddy, K.R.; Raghu, A.V. Polyaniline–fly ash nanocomposites synthesized via emulsion polymerization: Physicochemical, thermal and dielectric properties. *Mater. Sci. Energy Technol.* **2021**, *4*, 107–112. [CrossRef]
22. Singh, S.; Perween, S.; Ranjan, A. Dramatic enhancement in adsorption of congo red dye in polymer–nanoparticle composite of polyaniline–zinc titanate. *J. Environ. Chem. Eng.* **2021**, *9*, 105149. [CrossRef]
23. Minisy, I.M.; Salahuddin, N.A.; Ayad, M.M. Adsorption of methylene blue onto chitosan–montmorillonite/polyaniline nanocomposite. *Appl. Clay Sci.* **2021**, *203*, 105993. [CrossRef]
24. Beygisangchin, M.; Abdul Rashid, S.; Shafie, S.; Sadrolhosseini, A.R.; Lim, H.N. Preparations, Properties, and Applications of Polyaniline and Polyaniline Thin Films—A Review. *Polymers* **2021**, *13*, 2003. [CrossRef]
25. Zhang, Y.; Zhou, M.; Dou, C.; Ma, G.; Wang, Y.; Feng, N.; Wang, W.; Fang, L. Synthesis and biocompatibility assessment of polyaniline nanomaterials. *J. Bioact. Compat. Polym.* **2019**, *34*, 16–24. [CrossRef]
26. Perumal, A.; Kannan, S.; Nallaiyan, R. Silver nanoparticles incorporated polyaniline on TiO₂ nanotube arrays: A nanocomposite platform to enhance the biocompatibility and antibiofilm. *Surfaces Interfaces* **2021**, *22*, 1–13. [CrossRef]
27. Maruthapandi, M.; Saravanan, A.; Manohar, P.; Luong, J.H.T.; Gedanken, A. Photocatalytic Degradation of Organic Dyes and Antimicrobial Activities by Polyaniline–Nitrogen-Doped Carbon Dot Nanocomposite. *Nanomaterials* **2021**, *11*, 1128. [CrossRef]
28. Zhu, J.; Chen, J.; Zhuang, P.; Zhang, Y.; Wang, Y.; Tan, H.; Feng, J.; Yan, W. Efficient adsorption of trace formaldehyde by polyaniline/TiO₂ composite at room temperature and mechanism investigation. *Atmos. Pollut. Res.* **2021**, *12*, 1–11. [CrossRef]
29. Khong, C.H.; Teh, G.B.; Phang, S.W. Effect of Titanium Dioxide and Carbon Nanotubes on Polyaniline Nanocomposites for Heavy Metals Removal. In *POLYCHAR 25—World Forum on Advanced Materials*; De Gruyter: Berlin, Germany, 2018; Volume 382, pp. 1–8. [CrossRef]
30. Anjum, M.; Miandad, R.; Waqas, M.; Gehany, F.; Barakat, M. Remediation of wastewater using various nano-materials. *Arab. J. Chem.* **2019**, *12*, 4897–4919. [CrossRef]
31. Azizi-Lalabadi, M.; Ehsani, A.; Divband, B.; Alizadeh-Sani, M. Antimicrobial activity of Titanium dioxide and Zinc oxide nanoparticles supported in 4A zeolite and evaluation the morphological characteristic. *Sci. Rep.* **2019**, *9*, 17439. [CrossRef]
32. Parrino, F.; Palmisano, L. *Titanium Dioxide (TiO₂) and Its Applications*, 1st ed.; Elsevier: Cambridge, MA, USA, 2021; pp. 13–666. [CrossRef]
33. Fosso-Kankeu, E. *Nano and Bio-Based Technologies for Wastewater Treatment: Prediction and Control Tools for the Dispersion of Pollutants in the Environment*, 1st ed.; John Wiley & Sons: Hoboken, NJ, USA; Beverly, NJ, USA, 2019; pp. 147–330. [CrossRef]
34. Sato, N.; Aoyama, Y.; Yamanaka, J.; Toyotama, A.; Okuzono, T. Particle Adsorption on Hydrogel Surfaces in Aqueous Media due to van der Waals Attraction. *Sci. Rep.* **2017**, *7*, 6099. [CrossRef]
35. Leite, F.L.; Bueno, C.C.; Da Róz, A.L.; Ziemath, E.C.; Oliveira, O.N., Jr. Theoretical Models for Surface Forces and Adhesion and Their Measurement Using Atomic Force Microscopy. *Int. J. Mol. Sci.* **2012**, *13*, 12773–12856. [CrossRef] [PubMed]
36. Király, Z.; Turi, L.; Dékány, I.; Bean, K.; Vincent, B. Van der Waals attraction between Stöber silica particles in a binary solvent system. *Colloid Polym. Sci.* **1996**, *274*, 779–787. [CrossRef]
37. Tolias, P. Lifshitz calculations of Hamaker constants for fusion relevant materials. *Fusion Eng. Des.* **2018**, *133*, 110–116. [CrossRef]
38. Israelachvili, J.N. *Intermolecular and Surface Forces*, 3rd ed.; Elsevier Inc.: Amsterdam, The Netherlands; Academic Press: Burlington, NJ, USA, 2011; ISBN 978-0-12-375182-9.
39. Hamaker, H.C. The London–Van der waals attraction between spherical particles. *Physica* **1937**, *4*, 1058–1070. [CrossRef]
40. London, F. The general theory of molecular forces. *Trans. Faraday Soc.* **1937**, *33*, 8–26. [CrossRef]
41. Keesom, W.H. The cohesion forces in the theory of Van Der Waals. *Phys. Z.* **1921**, *22*, 129–141.
42. Debye, P. Molecular forces and their electric explanation. *Phys. Z.* **1921**, *22*, 302–308.
43. Lipkin, D.M.; Israelachvili, J.N.; Clarke, D.R. Estimating the metal–ceramic van der Waals adhesion energy. *Philos. Mag. A* **1997**, *76*, 715–728. [CrossRef]
44. Karkkainen, K.K.; Sihvola, A.H.; Nikoskinen, K.I. Effective Permittivity of Mixtures: Numerical Validation by the FDTD Method. *IEEE Trans. Geosci. Remote Sens.* **2000**, *38*, 1303–1308. [CrossRef]
45. Garnett, J.C.M. VII—Colours in Metal Glasses, in Metallic Films, and in Metallic Solutions—II; Series A Containing Papers of a Mathematical or Physical Character. *Philos. Trans. Royal Soc. Lond.* **1906**, *205*, 237–288.
46. Saravanan, S.; Mathai, C.J.; Anantharaman, M.R.; Venkatachalam, S.; Prabhakaran, P.V. Investigations on the electrical and structural properties of polyaniline doped with camphor sulphonic acid. *J. Phys. Chem. Solids* **2006**, *67*, 1496–1501. [CrossRef]
47. Dang, M.; Yongyao, L.; Kecheng, G.; Guiping, Z.; Renkuan, Y. Ellipsometric Spectra and Refractive Index of Polyaniline. *Chin. Phys. Lett.* **1993**, *10374*, 374–376. Available online: <http://iopscience.iop.org/0256-307X/10/6/016> (accessed on 17 September 2021).
48. Manke, F.; Frost, J.M.; Vaissier, V.; Nelson, J.; Barnes, P.R.F. Influence of a nearby substrate on the reorganization energy of hole exchange between dye molecules. *Phys. Chem. Chem. Phys.* **2015**, *17*, 7345–7354. [CrossRef] [PubMed]
49. Fernández, D.P.; Mulev, Y.; Goodwin, A.R.H.; Sengers, J.M.H.L. A Database for the Static Dielectric Constant of Water and Steam. *J. Phys. Chem. Ref. Data* **1995**, *24*, 33–70. [CrossRef]
50. Al-Ghamdi, A.; Al-Saigh, Z.Y. Surface and thermodynamic characterization of conducting polymers by inverse gas chromatography: I. Polyaniline. *J. Chromatogr. A* **2002**, *969*, 229–243. [CrossRef]

-
51. Govindaraj, Y.; Parida, S. Autogenous chemical and structural transition and the wettability of electropolymerized PANI surface. *Appl. Surf. Sci.* **2019**, *481*, 174–183. [[CrossRef](#)]
 52. Owens, D.K. Some thermodynamic aspects of polymer adhesion. *J. Appl. Polym. Sci.* **1970**, *14*, 1725–1730. [[CrossRef](#)]